Differential Cross Sections with Spin Analysis for $4\,^2S_{1/2} \rightarrow 4\,^2P_{1/2,3/2}$ Excitation of Potassium by Electrons*

Marvin Goldstein,† Abraham Kasdan, and Benjamin Bederson
New York University, New York, New York 10003
(Received 2 June 1971)

The atomic-beam recoil technique has been used to obtain the ratio of spin-flip to full differential cross sections, for $4\,^2S_{1/2} \rightarrow 4\,^2P_{1/2,3/2}$ excitation in potassium by electrons. Data are presented at energies of from 3 to 10 eV, and for electron scattering angles of from $\theta \approx 0°$ to 20°, in 5-deg intervals. Additional data at $\theta \approx 0°$, for energies from threshold to 20 eV, are also presented. Appropriate scattering amplitudes are calculated using the Born, Ochkur, and close-coupling approximations, and comparison with our experiments is made. Exchange is necessary to account for the $\theta \approx 0°$ data; the close-coupling results are in fair agreement with all of the angular data, while the Ochkur approximation gives good agreement at very small angles.

I. INTRODUCTION

A recent article by Rubin, Bederson, Goldstein, and Collins[1] (RBGC) presented a general discussion of the atomic-beam recoil technique as applied to the study of inelastic electron-atom collisions with spin analysis. In particular, the case of scattering by alkali atoms, neglecting nuclear spin, was considered. The RBGC article shows how to relate the observable of this experiment, which is the ratio of differential spin-flip cross section to full differential cross section, to the appropriate scattering amplitudes. The article also contains analyses of the effects of finite atom- and electron-beam energies and widths on the scattering signals.

A subsequent article by Collins, Bederson, and Goldstein[2] (CBG) discusses experimental results using this technique for *elastic* and *total* scattering of electrons by potassium. Differential, differential exchange, and total scattering cross sections were given, and comparison was made to two-state close-coupling calculations of Karule[3] (below the excitation threshold), and of Karule and Peterkop[4] (above the first excitation threshold). For all three types of measurements our results were in fair to good agreement with the close-coupling calculations. A far more sensitive test of the two-state close-coupling approximation would be the study of inelastic (nS-nP) collisions, to which a two-state close-coupling expansion could not be expected to converge as rapidly as it does for the elastic channel in the alkalis, where the induced electric dipole polarization potential dominates the elastic scattering, and the resonance transition nS-nP accounts for virtually all of the atomic polarizability.

We present here measurements of relative spin-flip cross sections attributable to nS-nP collisions in potassium; we believe these to be the first inelastic differential spin-flip cross sections to be reported.[5] Specifically, data have been obtained for the ratio of spin-flip to full differential cross sections, for electron scattering angles between 0° and 20°, and for energies between 3 and 10 eV, for the $4\,^2S_{1/2} \rightarrow 4\,^2P_{1/2,3/2}$ transitions in potassium. Additional data are also presented for small-angle scattering from threshold to 20 eV. The results are compared to the close-coupling calculations of Karule and Peterkop,[4] as well as to the Born and Ochkur approximations. In these latter comparisons it is important to note that for the relative data, that is, the ratio of spin-flip to full differential cross sections, the radial portions of the atomic wave functions cancel. The general forms of the Born and Ochkur approximations are tested, without need for accurate wave functions.

The principal improvement in the experimental setup over that described in RBGC is the added capability of allowing the electron gun to rotate about the axis of the atomic beam. This effectively permits analysis of the scattered atom beam out of the plane of scattering (defined as the plane which contains the electron and atom momenta), which in turn helps us to better discriminate against elastic and inelastic collisions other than $4S$-$4P$.

II. EXPERIMENTAL METHOD

The experimental technique, values of apparatus parameters, and operating characteristics of the apparatus are contained in the RBGC and CBG articles, to which the reader is referred for details. The rotational feature of the electron gun was added to assist in discrimination against spin-changing collisions resulting from scattering in other channels, particularly the elastic spin ex-

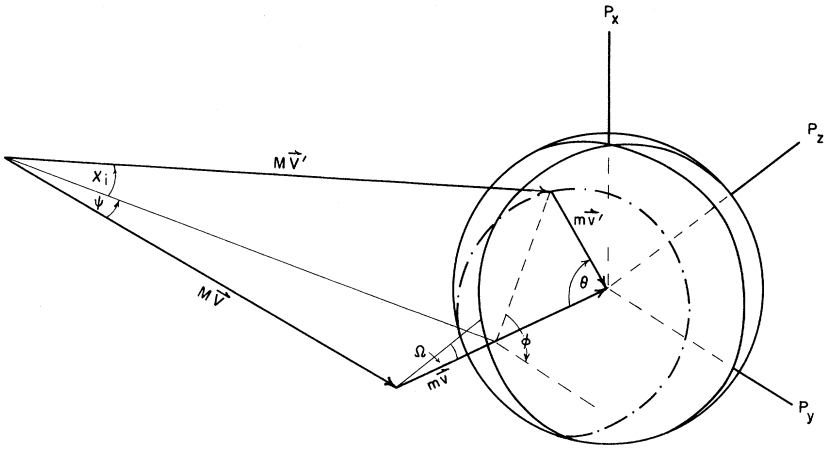

FIG. 1. Perspective view of momentum sphere for a particular inelastic channel (see text).

change. The operation of the rotatable electron gun is illustrated in Figs. 1 and 2, which represent simplified momentum diagrams.

Figure 1 shows the general momentum relations for cross-fired atom and electron beams. The directions of the momentum axes coincide with the x, y, z axes defined in our experiment as follows: x is the vertical direction, y is the direction of the undeflected atom beam, and z is the direction of displacement of the detector. In the present work, the incident electron beam is in the x-z plane and makes an angle Ω with the z direction; in past work Ω was zero. The initial and final atom and electron momenta are $M\vec{V}$, $m\vec{v}$ and $M\vec{V}'$, $m\vec{v}'$, respectively. To first order in m/M, $V = V'$ and $v' = [2(E - E_0)/m]^{1/2}$, where E and E_0 are the kinetic energy of the incident electron and the atomic excitation energy, respectively. We define a reference plane to be the plane containing the vector $m\vec{v}$ and the y axis. The atomic scattering angles are then defined as follows: ψ is the angle between $m\vec{v}$ and the projection of $M\vec{V}'$ in the reference plane; χ is the angle between this projection and $M\vec{V}'$.

θ, φ are the polar and azimuthal scattering angles. θ is measured with reference to the $m\vec{v}$ direction. φ is the angle between the plane formed by $m\vec{v}'$ and $m\vec{v}$, and the reference plane. Thus $\varphi = 0, \pi$ for scattering into the reference plane.

The surface of the momentum sphere represents the loci of the momenta of all electrons scattered with final energy $E - E_0$ and hence also the loci of the momenta of all atoms scattered into the final state of energy E_0. The loci of the final momenta of all atoms corresponding to electron polar scattering angle θ lie on the circle formed by the intersection of the momentum sphere and a cone of apex angle θ (the dot-dashed circle in Fig. 1). When $\Omega = 0$, the recoil angle ψ is a function of θ only, independent of φ, to the first order in mv'/MV. This enables a very simple transformation to be effected between ψ and θ, thereby obtaining relative differential cross sections without resort to complicated analysis of the scattered-beam deflection patterns. This is clearly still the case in the present work when $\Omega \neq 0$. However, relating electron scattering angles to atom scattering angles in the detector plane is more complicated here. In this paper, however, we only present *ratios* of spin-flip to full differential scattering and do not attempt to obtain relative cross-section curves;

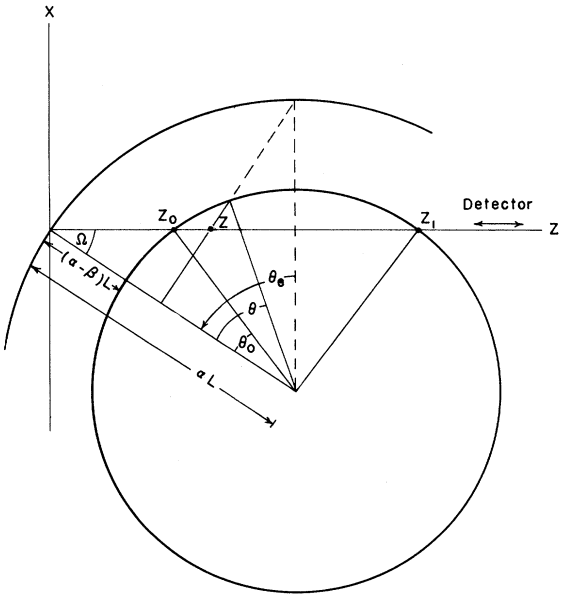

FIG. 2. Projection of great circle of momentum sphere in $P_x - P_z$ plane, transformed into displacement in plane made by direction of detector motion (z direction) and the vertical direction (x direction). Undeflected atom beam is at origin, moving out of paper (see text). θ_e is the polar scattering angle corresponding to elastically scattered atoms which arrive at z.

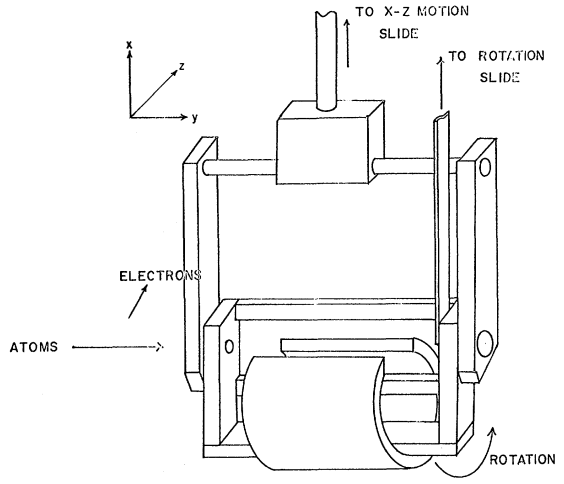

FIG. 3. Rotating gun mount. The gun itself (not shown) fits between the pole faces of the permanent magnet; both the gun and the magnet rotate together. The atom beam passes through the hollow pivot bearings.

as a consequence there is no need to present the full recoil analysis for the $\Omega \neq 0$ case. The two great circles shown in Fig. 1, which intersect on the P_x axis, are in the x-z and x-y planes, respectively. The corresponding elastic momentum sphere possesses the same origin as the inelastic sphere; its radius equals mv.

We wish to transform the x-z great circle into displacement in the detector plane, as shown in Fig. 2. Since ψ, χ are small these displacements are ψL and χL for the $m\vec{v}$ direction and for the direction perpendicular to $m\vec{v}$. The coordinate axes are the x and z axes (the atom beam is moving out of the paper). The origin of all the momenta circles is along the line making angle Ω with the z direction a distance αL from the coordinate origin, where $\alpha = mv/MV$. The radius of the inelastic circle is $\beta L = mv'/MV$ and the elastic circle is αL.

The position z_0 is the point at which the detector first intersects atoms which are inelastically scattered into the state E_0. z_1 is the corresponding detector position where it no longer intersects inelastically scattered atoms, while z is the detector position corresponding to the (general) polar angle θ. These quantities are obtained from the following relations:

$$\sin\theta_{0,1} = (\alpha/\beta)\sin\Omega[\cos\Omega \mp (\beta^2/\alpha^2 - \sin^2\Omega)^{1/2}], \quad (1)$$

$$z_{0,1} = \alpha L[\cos\Omega \mp (\beta^2/\alpha^2 - \sin^2\Omega)^{1/2}] , \quad (2)$$

$$z = (\alpha L - \beta L\cos\theta)/\cos\Omega , \quad (3)$$

with the $-$, $+$ signs referring to z_0, z_1, respectively.

In the present experiment z is varied with Ω kept fixed, and data are obtained as a function of z with and without the spin analyzer operative. The observable is $R(\theta)$, the ratio of scattering signal at θ [obtained using Eq. (3)] of atoms which have changed their spin state to the full scattering signal at θ. Thus we have

$$R(\theta) = \sigma_{SF}(\theta)/\sigma(\theta) , \quad (4)$$

where $\sigma_{SF}(\theta)$ is the spin-flip differential cross section at θ and $\sigma(\theta)$ is the full differential cross section at θ. By taking ratios of scattering signals at the same z, the complicated azimuthal form factors, which are functions of detector geometry and Ω, cancel. There remain, however, contributions of the elastically scattered atoms. That these could introduce a spin-exchange signal must be taken into account; this will be discussed in Sec. IV. The relation of $R(\theta)$ to the appropriate scattering amplitudes is discussed in Sec. V.

The gun design and its operating characteristics are described in detail elsewhere.[6] A sketch of the rotatable gun mount is shown in Fig. 3. The entire gun and magnetic field assembly (necessary to decouple nuclear and electronic spins in potassium) fits between the pole faces of the magnet as shown in Fig. 3. The atom beam passes through the hollow centers of the two pivot bearings, ensuring that the interaction volume is relatively unaffected as Ω is varied. (Although the beam overlap volume will of course change as Ω is varied, in the present *ratio* experiment this does not cause any error.) Separate gun motions for alignment and for rotation are available.

III. DATA ACQUISITION

The standard operating procedure employed in the $R(\theta)$ measurements was as follows: After reaching stable oven temperature (between 250 and 300 °C), the scattering-gun characteristics were determined. These included energy-distribution and absolute-energy determinations. The gun characteristics were checked periodically during each run to ensure that no changes had occurred. The quantities T_0 and D_0 were then determined. T_0 is the transmission factor of the E-H gradient spin analyzer (the ratio of the "fields-on" to "fields-off" beam at the maximum of the beam profile). D_0 is the residual depolarization of the atom beam, resulting from imperfect optics, scattering, etc., in the polarizer magnet. T_0 is of the order of 0.75 and D_0 of the order of 0.01–0.02. (See Appendix A of CBG for a discussion of the correction procedures.)

The inelastic scattering-in signals were obtained using a modulated electron scattering current and lock-in detection; these signals were digitalized in an analog-to-digital converter and integrated using a scalar timer. The integration times for each run varied according to the signal level; times of from

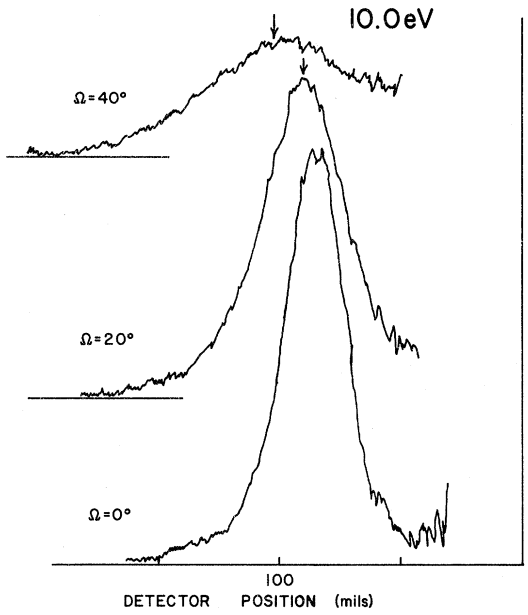

FIG. 4. Scattering-in beam profiles at 10 eV, for three orientations of electron gun ($\Omega = 0°$, 20°, and 40°). Vertical arrows on the $\Omega = 20°$ and 40° curves indicate the calculated positions of the onset of inelastic scattering.

6.0 min per counting period were used. The number of counting periods per point varied from a total of ten for high S/N to up to twenty for low S/N (defined as one run). The data, via IBM cards, were processed by computer to yield $R(\theta)$ and the statistical errors. In general, each run had an associated statistical error of no more than 5%. Most of the data were actually taken with Ω set to correspond to $\theta = 5°$, and by increasing z, i.e., by moving into the momentum sphere to obtain data for $\theta \geq 10°$. At least three runs were made at each angle and energy; these were usually made on different days under varying beam and gun operating conditions. The data thus obtained yielded the observed ratio $R_T(z)$, the uncorrected ratio of spin-flip to full scattering signal at z.

Some scattering-in beam profiles are shown in Fig. 4, for three orientations of the electron gun ($\Omega = 0°$, 20°, and 40°). Such curves, taken directly from the recorder plots, were obtained to ensure proper operation of the apparatus. The vertical arrows on the $\Omega = 20°$ and 40° curves indicate the expected positions of the scattering-in maxima, i.e., the positions of z_0 as calculated from Eq. (2).

IV. CORRECTIONS AND DISCUSSIONS OF ERRORS

We first correct for the imperfect transmission and residual depolarization, as discussed in Appendix A of CBG. This is done by applying Eq. (A4) of CBG modified by the inclusion of inelastic channels to the experimentally observed spin-flip ratio R_T at the detector displacement z, to obtain

$$R(z) \equiv \sum_l R_l(\theta_l) = [R_T(z) - D_0]/(T_0 - D_0) \quad . \tag{5}$$

The principal contribution to $R(z)$ is from the elastic channel (contributions of other inelastic channels are discussed below). Assuming for the moment that this is the case, $R(z)$ will have the form

$$R(z) = \frac{\gamma(\theta)\sigma_{SF}(\theta) + \gamma_e(\theta_e)\frac{1}{2}\sigma_{ex}(\theta_e)}{\gamma(\theta)\sigma(\theta) + \gamma(\theta_e)\sigma(\theta_e)} \quad , \tag{6}$$

where $\gamma(\theta)$ equals the azimuthal form factor (AFF) for inelastic scattering at θ; $\gamma_e(\theta_e)$ equals the AFF for elastic scattering at θ_e; $\sigma_{ex}(\theta_e)$ equals the elastic differential spin-exchange cross section; $\sigma(\theta)$ equals the full elastic differential cross section; and θ, θ_e are the electron polar scattering angles corresponding to the detector displacement z for inelastic and elastic scattering, respectively (see Fig. 2).

The factor $\frac{1}{2}$ in Eq. (6) arises because only half of all exchange events are observable, owing to the use of unpolarized electrons. Defining $\rho(\theta)$ as

$$\rho(\theta) = \sigma_{SF}(\theta)/\sigma(\theta) \quad , \tag{7}$$

and solving Eq. (6) for $\rho(\sigma)$, we obtain

$$\rho(\theta) = R(z) + \frac{\gamma_e(\theta_e)\sigma_e(\theta_e)}{\gamma(\theta)\sigma(\theta)} \left(R(z) - \tfrac{1}{2} \frac{\sigma_{ex}(\theta_e)}{\sigma_e(\theta_e)} \right) \quad . \tag{8}$$

The quantity in large parentheses on the right-hand side of Eq. (8) contains two corrections to $\rho(\theta)$. The first is the (positive) correction caused by the larger net scattering signal observed at z as a result of elastic scattering, which causes a smaller net spin-flip signal ratio. The second is the (negative) correction caused by the elastic spin-exchange signal, which results in an increased effective spin-flip signal ratio.

At the small scattering angles of this experiment ($\theta \leq 20°$), the first correction is substantially larger than the second, since $\frac{2}{9} < R < \frac{5}{9}$ (RBGC), while $\sigma_{ex}(\theta)/\sigma(\theta)$ is generally less than 0.1 for energies below threshold (CGB), and is likely to possess similar behavior at the above-threshold energies of the present work.[4] Thus, the relative error caused by elastic scattering is of the order of $\gamma_0\sigma_0/\gamma\sigma$ or less. This ratio is quite small, as a result of two factors. First, at small angles with the detector lying well within the elastic momentum sphere, the ratio of γ_0/γ is quite small. This is shown in Table I, which presents calculated ratios of γ_0/γ at small θ for energies between 3 and 10 eV, for $\Omega = 0°$. Ratios at finite though small Ω are similar. Second, the differential *inelastic* cross sections at the small angles of this experiment are

TABLE I. Ratios of elastic to inelastic AFF's corresponding to inelastic scattering angles of 0°–20°, $\Omega = 0°$.

Energy (eV)	$\gamma_e(\theta_e)/\gamma(\theta)$ $\theta = 0°$	5°	10°	15°	20°
3	0.0066	0.041	0.142	0.193	0.272
4	0.0066	0.043	0.194	0.280	0.368
5	0.0067	0.047	0.181	0.300	0.428
6	0.0066	0.051	0.200	0.352	0.500
7	0.0065	0.049	0.304	0.400	0.500
8	0.0065	0.055	0.272	0.500	0.500
9	0.0066	0.063	0.350	0.461	0.444
10	0.0065	0.045	0.350	0.500	0.545

substantially larger than the differential elastic cross sections at the appropriate inelastic angles θ, which correspond to the elastic scattering angle θ_e. The angles θ_r, as a function of θ for various energies and for Ω, are shown in Table II.

As a consequence of these two factors, the correction in R caused by elastic scattering can be assumed to be no more than several percent. Hereafter we shall use $R(\theta)$ and $\rho(\theta)$ interchangeably, since this error is generally substantially smaller than the statistical error.

The angular resolution is limited chiefly by (i) the velocity distribution of the atom beam, (ii) the energy spread of the electron beam, and (iii) the finite beam and detector widths. The polarizer magnet produces an atom beam with resolution $\Delta v/v \simeq 0.08$. The electron energy spread varied from about $\Delta E/E \simeq 0.1$ at 3 eV to up to 0.05 at 10 eV. (Other errors associated with the electron gun are discussed in CBG.) The beam height and width and detector width were all $\simeq 0.010$ in. All of these distributions combine to give an uncertainty in θ which is approximately 5°, being somewhat smaller at larger energies and angles, and larger at smaller energies and angles. (The AFF reduces these somewhat, although its effect has not been included in the resolution estimates.)

The finite angular resolution is simulated in our comparison of theory and experiment at $\theta \approx 0°$ (Sec. V) by averaging the theoretical estimates in the Born and Ochkur approximations over a Gaussian angular weighting factor centered at θ with half-width $\Delta\theta$. (This correction is not necessary at larger angles.)

TABLE II. Elastic scattering angles corresponding to inelastic scattering angles of 0°–20°, $\Omega = 0°$.

Energy (eV)	$\theta = 0°$	5°	10°	15°	20°
3	47	47	48	49.5	50.3
4	41.5	41.5	43	45	45.5
5	34.5	34.5	35	39	40
6	31	31	33	34	35
7	28.5	28.5	31	32	34
8	27	27	30	31	33
9	25	25	26	30	32
10	25	25	26	29	32

TABLE III. Detector displacement (in mils) for appearance of 10°, 15°, 20° scattering into $4P$, and for appearance of 0° (onset) scattering into $5S$, $5P$.

Energy (eV)	($\Omega = 0°$) 10°($4P$)	15°($4P$)	20°($4P$)	0°($5S$)	0°($5P$)
3	201	208	220	385	•••
4	170	181	195	301	393
5	158	170	189	269	343
6	149	165	185	247	310
7	143	161	186	231	288
8	142	162	190	226	279
9	144	167	199	227	281
10	144	169	206	225	278

At the energies and angles studied in the present experiment, contributions of other inelastic channels can be seen to be quite small (apart from the substantially smaller cross-section magnitudes involved.) The three closest levels which could possibly contribute to spin-flip signals are $5S$, $3D$, and $5P$, which are excited at 2.61, 2.67, and 3.1 eV, respectively. Table III shows the detector position z at which 10°, 15°, and 20° scattering appear for the $4P$ state, compared to the position at which 0° scattering for $5S$ and $5P$ appears ($3D$ is intermediate between these two cases). (0° and 5° positions for $4P$ are even smaller, and hence even better separated from $5S$, $3D$, and $5P$ onset.)

With 0.010-in. beam and detection widths, it is seen that other excitation channels are easily discriminated against even with the detector well inside the $4P$ momentum sphere.

The data are presented in Figs. 5–9, along with comparison with theory, which is discussed in Sec. V. Figures 5–8 show the angular distribution data for energies ranging from 3 to 10 eV. Figure 9 shows data taken at nominally 0° from threshold to 20 eV. The vertical error bars are statistical errors (two standard deviations). Systematic errors are discussed in Sec. V.

V. COMPARISON WITH THEORY

We have shown[7,8] that the observed ratio $R(\theta)$ is given by

$$R(\theta) = \frac{4}{9} + \left(\frac{10|g_1|^2 + |g_0|^2 - 8\sigma_1(\theta)}{8\sigma(\theta)} \right) , \quad (9)$$

where $\sigma(\theta)$ is the "full" differential cross section

$$\sigma(\theta) = \tfrac{1}{2}(|f|^2 + |g|^2 + |f-g|^2) , \quad (10)$$

f, g are the direct and the exchange scattering amplitudes, and the subscripts 1, 0 refer to $S \rightarrow P$ excitation with magnetic quantum number of the excited state $M_l = 1, 0$, respectively.

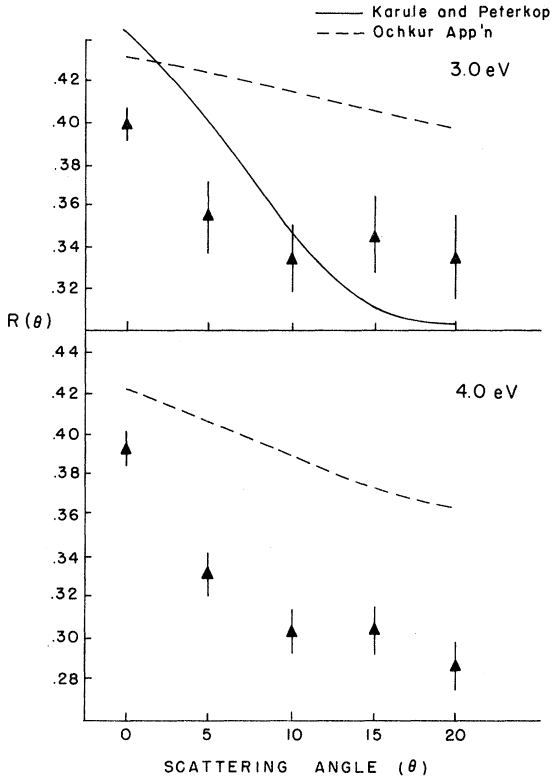

FIG. 5. $R(\theta)$, the ratio of spin-flip to full differential scattering cross sections for $4\,^2S_{1/2}$-$4\,^2P_{1/2,3/2}$ excitation of potassium by 3- and 4-eV electrons. Comparison is to Ochkur approximation (hollow triangles) at 3 and 4 eV, and to close-coupling calculations at 3 eV. Error bars on data represent statistical error only (see text for discussion of angular resolution).

Here we show how to obtain the appropriate amplitudes and cross sections for the Born, Ochkur, and close-coupling approximations. As a starting point for the Born and Ochkur approximations we use the general expression for the direct scattering amplitude, valid for a one-electron atom, [9]

$$f(\theta,\varphi;n_0l_0m_0\to nlm) = \frac{-2me^2}{\hbar^2K}\int \psi^*_{nlm}(\vec{r})e^{i\vec{K}\cdot\vec{r}}\,\psi_{n_0l_0m_0}(\vec{r})\,d\vec{r}\ , \quad (11)$$

referred to the $\vec{K}$ axis (i.e., $\vec{K}$ is the quantization axis), where $\vec{K}=\vec{k}-\vec{k}_0$ with $\vec{k}$, $\vec{k}_0$ the final and initial wave vectors of the free electron, $\vec{r}$ is the position vector of the atomic electron, and $nlm, n_0l_0m_0$ refer to the set of final and initial quantum numbers of the target atom. The polar scattering angle θ and the angle β [see Eqs. (14) and (15)] are defined in Fig. 10.

For an ns-np excitation we can write

$$\psi_{nl_0m_0}(\vec{r}) = R_{n0}(r)\ ,$$

$$\psi_{nlm}(\vec{r}) = R_{nl}(r)\,P_l^m(\cos\theta)\,e^{im\varphi}\ ,$$

so that Eq. (11) can be rewritten as

$$f(\theta,\varphi;n00\to nlm) = -\frac{2me^2}{\hbar^2K^2}\left(\int R_{nl}(r)R_{n0}(r)P_l^m(\cos\theta)\,r^2dr\sin\theta\,d\theta\right)\delta_{0m}\ , \quad (12)$$

where we have used the identity

$$\int_0^{2\pi} e^{im\phi}\,d\varphi = \delta_{0m}\ .$$

Note that $f\neq 0$ only if $m=0$, referred to the $\vec{K}$ axis. We now transform to the laboratory z axis, which is the $\vec{k}_0$ direction, using the usual rotational transformation matrices, [10] to obtain

$$|f(\theta,\varphi;\,n00\to n11)|^2 \equiv |f_1|^2 = \tfrac{1}{2}\sin^2\beta\ C\ , \quad (13)$$

$$|f(\theta,\varphi;\,n00\to n10)|^2 \equiv |f_0|^2 = \cos^2\beta\ C\ , \quad (14)$$

where C represents the r, θ integrations.

We first set $|g_0|$, $|g_1|$ equal to zero in Eq. (5) (i.e., we neglect exchange) and rewrite it, recalling that $\sigma(\theta)=\sigma_0(\theta)+2\sigma_1(\theta)$, to obtain

$$R(\theta) = \frac{4}{9}\left(\frac{|f_0|^2+|f_1|^2}{|f_0|^2+2|f_0|^2}\right)\ , \quad (15)$$

and now substitute Eqs. (13) and (14) into Eq. (15) to obtain the final expression for $R(\theta)$ in the Born

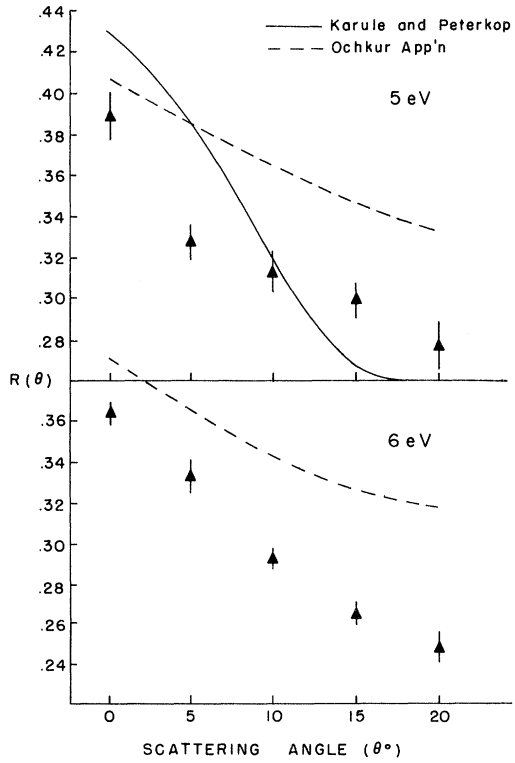

FIG. 6. Same as Fig. 5, for energies of 5 and 6 eV.

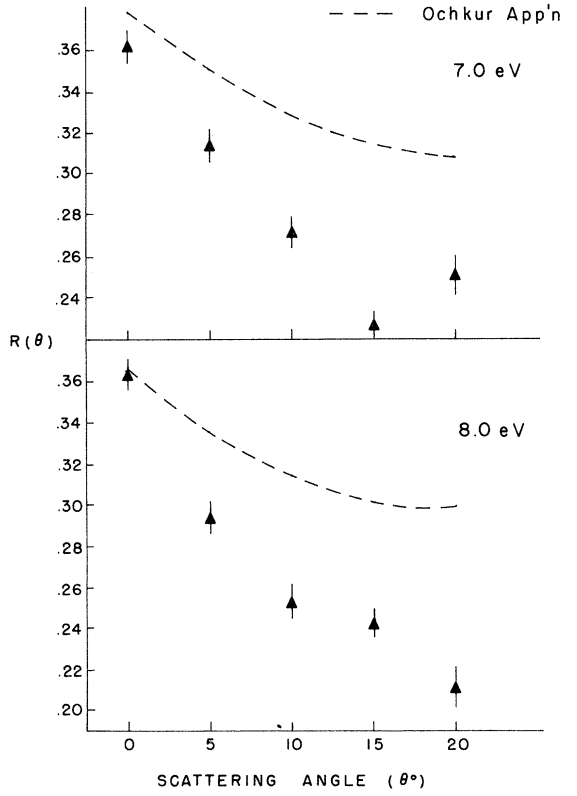

FIG. 7. Same as Fig. 5, for energies of 7 and 8 eV.

approximation without exchange,

$$R(\theta)=\frac{4}{9}\left(1-\frac{(E-E_0)\sin^2\theta}{2\{2E-E_0-2[E(E-E_0)]^{1/2}\cos\theta\}}\right), \tag{16}$$

where we have written k, k_0 in terms of the incident electron energy E and the excitation energy E_0.

The Ochkur approximation[10,11] is a Born approximation with exchange, in which the exchange integrals are evaluated by use of an expansion in powers of k_0 to obtain exchange amplitudes which are always proportional to the product of the direct amplitude and the ratio k^2/k_0^2, i.e.,

$$g\sim(k^2/k_0^2)f\ ,$$

with the proportionality the same for the 1, 0 states. We can therefore use Eq. (5) with exchange terms, noting that the proportionality constant cancels in numerator and denominator of the second term, and obtain

$$R(\theta)=\frac{\frac{4}{9}+\frac{1}{18}\{x^2+[(x-4)/x](1-E_0/E)\sin^2\theta\}}{(1-x+x^2)}\ , \tag{17}$$

where $x=2-E_0/E-2(1-E_0/E)^{1/2}\cos\theta$.

One does not obtain cancellation of the r, θ integrals when using the Born-Oppenheimer approximation—explicit evaluation of various exchange integrals is required. We have not attempted to perform these integrations, as the additional effort does not appear to be warranted here.

We now discuss the appropriate close-coupling expressions. The singlet (+) and triplet (−) scattering amplitudes for an $s\rightarrow p$ transition are given by[12,13]

$$f^{\pm}(\theta,\varphi;n_0 00\rightarrow nlm)=(\pi/kk_0)^{1/2}\sum_L C^{1,L+1,L}_{m,-m,0}\,Y^{-m}_{L+1}T^{\pm L}_{12}$$
$$-C^{1,L-1,L}_{m,-m,0}\,Y^{-m}_{L-1}\,T^{\pm L}_{13}(2L+1)^{1/2}\ , \tag{18}$$

where the C's are Clebsch-Gordan coefficients; the Y's are associated spherical harmonics; $T_{12}^{\pm L}$ is the Lth partial singlet or triplet T-matrix element, where total angular momentum of atom + free electron $= L+1$; and $T_{13}^{\pm L}$ is the T-matrix element corresponding to total angular momentum of atom + free electron $= L-1$. The singlet and triplet amplitudes and f, g are related by

$$f=\tfrac{1}{2}(f^{+}+f^{-})\ , \tag{19a}$$

$$g=\tfrac{1}{2}(f^{+}-f^{-})\ . \tag{19b}$$

The real and imaginary parts of the T matrix are obtained from the real R matrix (called the K matrix by Karule and Peterkop), whose elements for $L\leq 3$ are given in Ref. 4. We have calculated $R(\theta)$ using Eqs. (16)–(18). Except very close to

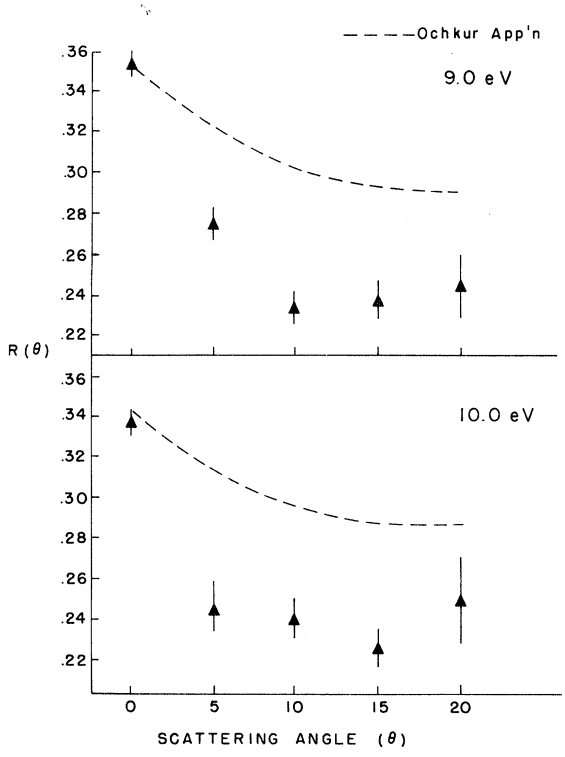

FIG. 8. Same as Fig. 5, for energies of 9 and 10 eV.

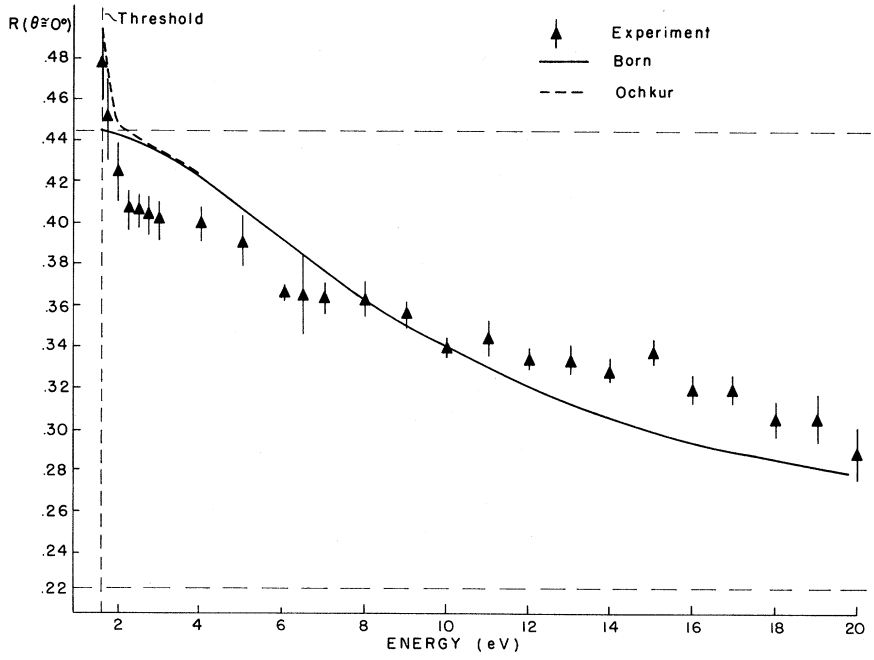

FIG. 9. $R(\theta)$ vs energy, for θ nominally 0°. The Born and Ochkur approximations are shown by dashed and by solid lines (both are essentially identical above about 2.5 eV). The finite angular resolution has been taken into account by folding a Gaussian angular weighting function of width 5° into the theoretical calculations. The two horizontal dashed lines represent the theoretical limit of $\frac{4}{9}$ (without exchange) and the high-energy limit of $\frac{2}{9}$.

threshold, the Born and Ochkur approximations give very nearly identical results; we show only the Ochkur approximation in our comparison with experiment. The close-coupling calculations have only been performed at 3, 4, and 5 eV, and we therefore cannot make a comparison at the higher energies at which measurements were made; comparison with Karule and Peterkop is shown in Figs. 5 and 6, since we have only the extended (unpublished) T elements for energies of 3 and 5 eV.[14]

Figure 9 shows $R(\theta)$ for θ nominally 0°. The Born and Ochkur approximations are weighted with a Gaussian smoothing function of 5° width, so as to approximate the angular resolution of our experiment. It can be seen that except close to threshold, the Born and Ochkur approximations give virtually identical results. The upper and lower horizontal lines at $R=\frac{4}{9}$ and $\frac{2}{9}$ are the threshold and high-energy limit for $R(\theta)$, neglecting exchange (RBCG). The threshold limit can be as high as $\frac{5}{9}$, for $g_0 \gg f_0$. It can be seen that there is a substantial exchange contribution close to threshold, which is well accounted for in the Ochkur approximation.

In all cases it is seen that while the Ochkur approximations give reasonable agreement with experiment at small angles, the agreement becomes poor for $\theta \approx 10°$ or greater. The close-coupling results are in substantially better agreement with experiment for all angles studied.

VI. CONCLUSIONS

This paper is the first to report differential excitation cross sections with spin analysis. We believe that substantial refinements in the recoil technique can be made, particularly by improving the energy and spatial resolutions of the atom and electron beams, and we are currently attempting such a refinement program at our laboratory, as well as extending our measurements to lithium and sodium. The pioneering close-coupling calculations of Karule and Peterkop seem to offer a very encouraging approach to the electron-atom collision problem, at least for the alkali metals. It is not reasonable to expect quantitative agreement with these calculations, in light of both the experimental uncertainties involved and the fact that only s and p states were included in the calculation. We would like very much to see more computational effort put into this problem, since it offers a fruitful meeting ground for critical comparison of theory and experiment. Such calculations for the lighter alkalis (lithium and sodium) have already been undertaken by Burke and Taylor[15] and by Norcross.[16] These calculations reveal some interesting structure at very low energies, which can in principal be reached by the recoil technique.

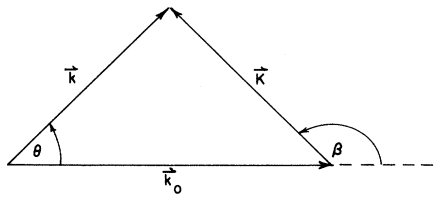

FIG. 10. Geometric relation of $\vec{k}_0$, $\vec{k}$, and $\vec{K}$.

ACKNOWLEDGMENTS

We wish to thank Professor H. H. Brown and Professor T. M. Miller for their invaluable assistance throughout the course of the experiment. We also gratefully acknowledge the help of our electronics engineer J. DeSantis and of the graduate students in the Atomic Beams and Plasma Physics Laboratory at New York University, Dr. Robert Celotta, Dr. H. Schwartz, R. Molof, R. Pai, and F. Murray.

---

*Work supported by the Air Force Office of Scientific Research, the Army Research Office, Durham, and the National Science Foundation.

†From a Ph. D. thesis by Marvin Goldstein in partial fulfillment of the requirements for the Ph. D. degree at New York University. Present address: Bell Telephone Laboratories, Whippany, N. J. 07981.

[1]K. Rubin, B. Bederson, M. Goldstein, and R. E. Collins, Phys. Rev. 182, 201 (1969).

[2]R. E. Collins, B. Bederson, and M. Goldstein, Phys. Rev. A 3, 1976 (1971).

[3]E. M. Karule, in University of Colorado JILA Information Center Report No. 3, 1966, p. 29 (unpublished) [English translation of *Atomic Collisions III*, edited by Y. Ia. Veldre (Latvian Academy of Sciences, Riga, 1965)].

[4]E. M. Karule and R. K. Peterkop, in Ref. 3, p. 1.

[5]Preliminary reports of this work have been presented at DEAP Conference, Seattle, 1970 (unpublished), and in the Proceedings of the VII International Conference on the Physics of Electronic and Atomic Collisions, Amsterdam, 1971 (unpublished).

[6]R. E. Collins, B. B. Aubrey, P. N. Eisner, and R. Celotta, Rev. Sci. Instr. 41, 1403 (1970).

[7]See Ref. 1, also B. Bederson, *Comments on Atomic and Molecular Physics* (Gordon and Breach, New York, 1971), Vol. 2, p. 160.

[8]A general discussion of relation of observables to scattering amplitudes is contained in Appendix A of Ref. 1, and in a recent article by H. Kleinpoppen [Phys. Rev. A 3, 2015 (1971)].

[9]B. Moiseiwitsch and S. J. Smith, Rev. Mod. Phys. 40, 238 (1969).

[10]D. Bohm, *Quantum Theory* (Prentice-Hall, Englewood Cliffs, N. J., 1951), p. 327 ff.

[11]V. I. Ochkur, Zh. Eksperim. i Teor. Fiz. 45, 734 (1963) [Sov. Phys. JETP 18, 503 (1964)].

[12]I. C. Percival and M. J. Seaton, Proc. Cambridge Phil. Soc. 53, 654 (1957).

[13]M. J. Seaton, in *Atomic and Molecular Processes*, edited by D. R. Bates (Academic, New York, 1962), Chap. 11.

[14]We are indebted to Dr. Karule for supplying us with R-matrix elements for $4 \leq L \leq 8$. Exchange was not included for these elements.

[15]P. G. Burke and A. J. Taylor, J. Phys. B 2, 869 (1969).

[16]D. W. Norcross (unpublished).

PHYSICAL REVIEW A VOLUME 5, NUMBER 2 FEBRUARY 1972

Theoretical Study of Generalized Oscillator Strengths in Atoms: Comparison with Experiment and Other Calculations

Steven Trent Manson
Department of Physics, Georgia State University, Atlanta, Georgia 30303
(Received 27 August 1971)

A central-field approximation is used to calculate generalized oscillator strengths (GOS) for a number of discrete and continuous transitions in the noble gases, the alkalis, and Hg, where experimental data exist. The comparisons show that this approximation yields good agreement with experiment except for the first few discrete excitations in low-Z and certain high-Z elements, and in the region of large peaks near threshold in continuum transitions. The reasons for the discrepancies are pointed out, in terms of the approximations made, and the usefulness of this type of calculation is discussed.

I. INTRODUCTION

The generalized oscillator strength (GOS) of an atom or molecule is the essential factor in the differential cross section for inelastic scattering of sufficiently fast charged particles[1-3] by that atom or molecule. A knowledge of the details of these inelastic cross sections is of vital importance in a number of areas, including space and atmospheric physics, plasma physics, astrophysics, radiation physics, and the penetration of charged particles into matter. In view of the importance of the GOS, it is unfortunate that, except for discrete excitations in helium, only a few isolated calculations and measurements have been reported. In an effort to remedy this situation, we have embarked on an extensive program of calculating the GOS for both discrete and continuum excitations of atoms throughout the periodic system. This study is being carried out for a threefold purpose: first, to obtain infor-